

DEEP LUMINOSITY FUNCTIONS OF OLD AND INTERMEDIATE-AGE GLOBULAR CLUSTERS IN NGC 1316: EVIDENCE FOR DYNAMICAL EVOLUTION OF SECOND-GENERATION GLOBULAR CLUSTERS¹

PAUL GOUDFROOIJ, DIANE GILMORE, AND BRADLEY C. WHITMORE
Space Telescope Science Institute, 3700 San Martin Drive, Baltimore, MD 21218

AND

FRANÇOIS SCHWEIZER
Carnegie Observatories, 813 Santa Barbara Street, Pasadena, CA 91101

Accepted by *ApJ Letters*

ABSTRACT

The Advanced Camera for Surveys on board the *Hubble Space Telescope* has been used to obtain deep high-resolution images of the giant early-type galaxy NGC 1316 which is an obvious merger remnant. These observations supersede previous, shallower observations which revealed the presence of a population of metal-rich globular clusters of intermediate age (~ 3 Gyr). We detect a total of 1496 cluster candidates, almost 4 times as many as from the previous WFPC2 images. We confirm the bimodality of the color distribution of clusters, even in $V-I$, with peak colors 0.93 and 1.06. The large number of detected clusters allows us to evaluate the globular cluster luminosity functions as a function of galactocentric radius. We find that the luminosity function of the inner 50% of the intermediate-age, metal-rich ('red') population of clusters differs markedly from that of the outer 50%. In particular, the luminosity function of the inner 50% of the red clusters shows a clear flattening consistent with a turnover that is about 1.0 mag fainter than the turnover of the blue clusters. This constitutes the first direct evidence that metal-rich cluster populations formed during major mergers of gas-rich galaxies can evolve dynamically (through disruption processes) into the red, metal-rich cluster populations that are ubiquitous in 'normal' giant ellipticals.

Subject headings: galaxies: star clusters — galaxies: elliptical and lenticular — galaxies: individual (NGC 1316) — galaxies: interactions

1. INTRODUCTION

Recent deep imaging studies of 'normal' giant elliptical galaxies with the *Hubble Space Telescope* (*HST*) and large, ground-based telescopes have shown that these galaxies usually contain rich globular cluster (GC) systems with bimodal color distributions (e.g., Kundu & Whitmore 2001; Larsen et al. 2001). Typically, roughly half of the GCs are blue, and half red. Follow-up spectroscopy with 8-m class telescopes revealed that both 'blue' and 'red' GC subpopulations are typically old ($\gtrsim 8$ Gyr, Forbes et al. 2001; Cohen, Blakeslee, & Côté 2003) implying that the bimodality is mainly due to differences in metallicity. The colors of the 'blue' GCs are usually similar to those of metal-poor halo GCs in the Milky Way and M31, while the mean colors of the 'red' GCs are similar to those of the diffuse light of their host galaxies (e.g., Geisler, Lee, & Kim 1996; Forbes, Brodie, & Grillmair 1997). Hence, the nature of the 'red', metal-rich GCs is likely to hold important clues to the star formation history of their host galaxies.

One environment *known* to produce metal-rich GCs and bimodal color distributions is that of vigorous starbursts induced by mergers of gas-rich galaxies. Massive young GCs have been commonly found in mergers and young merger remnants using *HST* observations (e.g., Holtzman et al. 1992; Schweizer 2002, and references therein). Follow-up spectroscopy has confirmed the ages (and in one case even the high masses, Maraston et al. 2004) of these young clusters predicted from their colors and luminosities (e.g., Zepf et al.

1995; Schweizer & Seitzer 1998). Their metallicities tend to be near solar, as expected for clusters formed out of enriched gas in spiral disks. A natural interpretation of these data is that the metal-rich GCs in 'normal' giant ellipticals formed in gas-rich mergers at $z \gtrsim 1$, and that the formation process of giant ellipticals with significant populations of metal-rich GCs was similar to that in galaxy mergers observed today (e.g., Schweizer 1987; Ashman & Zepf 1992).

However, one important, hitherto unsurmounted hurdle for this 'formation by merger' scenario has been the marked difference in the luminosity functions (hereafter LFs) of old vs. young GC systems (e.g., van den Bergh 1995). The LFs of old GC systems of 'normal' galaxies are well fit by Gaussians peaking at $M_V^0 \simeq -7.2$ mag with a dispersion of $\sigma \simeq 1.3$ mag (e.g., Whitmore 1997), while young GC systems in mergers and young remnants have power-law LFs with indices of $\alpha \simeq -2$ (e.g., Whitmore et al. 1999). Recent calculations of dynamical evolution of GCs (including two-body relaxation, tidal shocking, and stellar mass loss) show that the least massive GCs disrupt first as galaxies age, which can gradually transform the initial power-law LFs into LFs with Gaussian-like peaks or turnovers (e.g., Fall & Rees 1977; Baumgardt 1998; Fall & Zhang 2001; but see Vesperini 2001). Observational evidence of this effect has been reported for a GC system near the center of M 82, featuring a very short GC disruption timescale (de Grijs, Bastian, & Lamers 2003).

Intermediate-age merger remnants with ages of 1–5 Gyr are ideal probes for studying the long-term dynamical effects on GC systems formed during a major merger. Such galaxies are still identifiable as merger remnants through their morphological fine structure (e.g., Schweizer & Seitzer 1992), yet are old enough to ensure that substantial dynamical evolution of the globular clusters has already occurred.

Electronic address: goudfroi@stsci.edu

¹ Based on observations with the NASA/ESA *Hubble Space Telescope*, obtained at the Space Telescope Science Institute, which is operated by AURA, Inc., under NASA contract NAS5–26555.

Recent *HST* studies of candidate intermediate-age merger remnants have revealed that their ‘red’ GC subpopulations show LFs consistent with power laws (as expected if formed during a recent merger event; Goudfrooij et al. 2001b; Whitmore et al. 2002). However, the completeness limits of those studies were not faint enough to allow a detection of a turnover in the LFs. This *Letter* reports on new observations of the intermediate-age merger remnant NGC 1316 using the Advanced Camera for Surveys (*ACS*), installed on *HST* in March 2002, whose unprecedented sensitivity allows us, for the first time, to detect these turnovers.

2. NGC 1316

NGC 1316 is a prime example of an intermediate-age merger remnant. Extensive optical observations showed that NGC 1316 is a typical Morgan D-type galaxy with a surface brightness profile following an $r^{1/4}$ law (Schweizer 1980, 1981). Its outer envelope includes several non-concentric arcs, tails and loops that are most likely remnants of tidal perturbations, while the inner part of the spheroid is characterized by a surprisingly high central surface brightness and small effective radius for the galaxy’s luminosity. All of these features are consistent with NGC 1316 being the product of a dissipative merger with incomplete dynamical relaxation. Recently, Goudfrooij et al. (2001a; 2001b) discovered a significant population of ~ 3 Gyr old GCs of near-solar metallicity through a comparison of *BVIJHK* colors as well as $H\alpha$ and Ca II-triplet line strengths with population synthesis model predictions.

In the following we adopt a distance of 22.9 Mpc for NGC 1316 (see Goudfrooij et al. 2001b, hereafter Paper I).

3. OBSERVATIONS AND DATA ANALYSIS

NGC 1316 was observed with *HST* on March 4 and 7, 2003, using the wide-field channel of *ACS* and the F435W, F555W, and F814W filters, with total exposure times of 1860 s, 6980 s, and 4860 s, respectively. In this *Letter* we concentrate on the F555W and F814W images, which reach significantly deeper than the F435W image. The final F555W and F814W images were constructed from long (18–21 min) exposures at 4 or 6 dither positions, supplemented by a few short exposures to avoid saturation of the central regions. The individual images in each band were combined using the task MULTIDRIZZLE within IRAF/STSDAS v3.2. Saturated pixels in the long exposures were replaced by those in the short exposures while running MULTIDRIZZLE by setting the appropriate data quality flag in the affected pixels of the long exposures. The high sensitivity of the *ACS* images allowed us to reach about 1.9 mag deeper than the *WFPC2* images used in Paper I did.

WFPC2 images were taken in parallel to the *ACS* observations, $\sim 5'5$ away from the *ACS* pointings, in order to provide estimates for the number density of compact background galaxies and foreground stars as a function of brightness and color (see Sect. 4). The *WFPC2* exposures consisted of a total of 5100 s in F555W and 3000 s in F814W. Each set of *WFPC2* images was also combined using MULTIDRIZZLE.

The cluster selection procedure followed the one described in Paper I, to which we refer the reader interested in details. Briefly, we first built smooth galaxy model images from the combination of an isophotal model composed of pure ellipses and a median-filtered version of the image. The objects were then selected by applying the DAOFIND task from the DAOPHOT package (Stetson 1987) to an image prepared by dividing the F555W image by the square root of the corresponding model image (thus having uniform shot noise characteris-

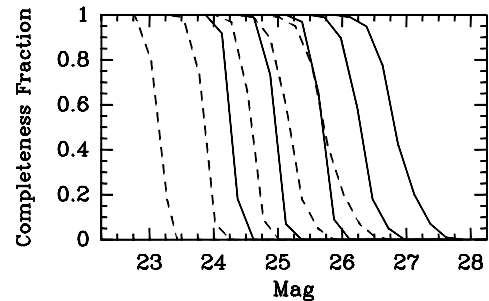


FIG. 1.— Completeness functions used for the *ACS*/*WFC* photometry of NGC 1316 GC candidates. Lines (solid for *V* band, dashed for *I* band) are shown for five background levels: From left to right: 1600, 800, 320, 200, and $140 \text{ e}^- \text{ pixel}^{-1}$ for an exposure time of 1100 s.

tics over the whole image). The detection threshold was set at 3σ above the background. Detections located within or on the edge of the dust features in NGC 1316 were excluded from the sample. As the resolution of the drizzled *ACS* images is high enough to resolve typical GCs at the distance of NGC 1316, a further subselection was made by restricting a ‘concentration index’ (the difference in magnitudes measured using radii of 2 and 5 pixels) to stay between 0.35 and 0.75 mag. This effectively filtered out extended background galaxies as well as bright foreground stars and any remaining hot pixels. Aperture corrections were $-0.49 (\pm 0.01)$ mag in *V* and $-0.56 (\pm 0.01)$ mag in *I* for an aperture radius of 3 *WFC* pixels (i.e., $0''.15$). These values were determined through measurements of several isolated, well-exposed GC candidates located throughout the field. The transformation of the instrumental magnitudes to Johnson/Cousins *V* and *I* was performed using the calibrations derived by the *ACS* Instrument Definition Team (Sirianni et al., in preparation).

Completeness corrections were performed for five background levels and several magnitude intervals by adding artificial objects (in batches of 300) with a radial intensity profile derived from a fit to real GC candidates in each frame (using DAOPHOT routines). The object colors were set equal to the median color of GC candidates. Figure 1 shows the resulting completeness functions.

4. TWO SUBPOPULATIONS AND THEIR LUMINOSITY FUNCTIONS

The top panel of Figure 2 depicts the *V* versus *V*–*I* color-magnitude diagram (hereafter CMD) for GCs in NGC 1316. The *V*–*I* colors of the GCs that are more luminous than any GC in the Milky Way are quite uniform and lie somewhat redward of the range covered by the Milky-Way halo GCs. Goudfrooij et al. (2001a) analyzed spectra of three of these bright GCs, and found all three to be \sim coeval with an age of 3.0 ± 0.5 Gyr and a solar metallicity (to within ± 0.15 dex). The fainter part of the CMD reveals a population of GCs with colors and luminosities that are consistent with those of halo GCs in our Galaxy (taken from the database of Harris 1996), as well as a larger population with a mean color that is consistent with those of the aforementioned brightest, metal-rich GCs throughout the sampled range of luminosities. As to the potential effect of dust extinction within NGC 1316, our selection criteria seem to have rendered the number of GC candidates with colors redder than expected (given the photometry errors) negligible regarding the discussion below.

The *V*–*I* color distribution of the GC candidates is shown in the bottom panel of Figure 2, for two brightness cuts. The bimodality appears more pronounced than in Paper I, and is

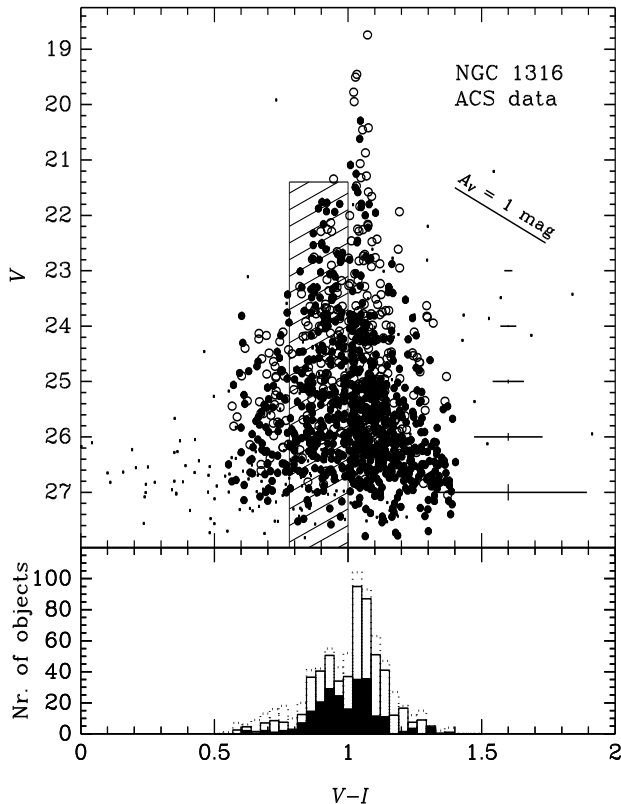


FIG. 2.— *Top panel:* V vs. $V-I$ color-magnitude diagram for compact sources in NGC 1316. Circles represent GC candidates, while dots represent foreground star candidates, i.e. objects with concentration parameters (see text) that are consistent with that of the ACS/WFC point spread function. The inner 50% of the GC candidates are shown as open circles, while the outer 50% are shown as filled circles. The hatched region represents the magnitude and color range for GCs in the Milky Way halo, placed at the distance of NGC 1316. Representative error bars are shown on the right-hand side of the diagram. The tilted line shows the reddening vector for $A_V = 1$ mag of extinction. *Bottom panel:* $V-I$ color distribution for GC candidates in NGC 1316, showing all GCs with $V \leq 26$ (open histogram), and GCs with $V \leq 24.5$ (filled histogram). The dashed lines represent GCs with $V \leq 26$ before correction for contamination by compact background galaxies.

clearly present down to $V = 26$ where the typical uncertainty in $V-I$ is ± 0.12 mag. Prior to creating this diagram, the color histogram of candidate GCs was corrected for contamination by compact background objects. This correction was derived from the list of compact objects detected in the three WF chips of the parallel, drizzled WFPC2 images, selected according to the same criteria as the GC candidates in the ACS images. The color distribution of the objects in the WFPC2 images was smoothed with a three-bin kernel to diminish small-number noise and scaled to the area of the ACS image prior to subtraction from the ACS color histogram. The effect of this correction is shown in Figure 2.

The luminosity functions of the blue and red GC subpopulations are shown in Figure 3, and were determined as follows. We first separated the GC candidates into ‘blue’ ($0.55 \leq V-I \leq 0.97$) and ‘red’ ($1.03 \leq V-I \leq 1.40$) subsamples. We avoided the overlapping region ($0.97 < V-I < 1.03$) to minimize the mixing of the two subsamples. A completeness correction was then applied to each GC by dividing its count of 1 by the completeness fraction corresponding to its brightness and background level. The latter fraction was calculated from the functions shown in Fig. 1, using bilinear interpolation in $\log(\text{background})$ space. The LFs were further

corrected for contamination by compact background objects using the smoothed and scaled LF of the objects in the parallel WFPC2 images, as described in the previous paragraph. The corrected LFs are shown as solid lines in Fig. 3, whereas the raw, ‘observed’ LFs are shown as dotted lines.

As found in Paper I, the LFs of the (full) blue and red GC subsystems in NGC 1316 are dramatically different from each other. The shape of the LF of the blue GC system is consistent with that for GCs in ‘normal’ galaxies and peaks near the expected turnover magnitude of $M_V = -7.2$. In contrast, the LF for the red GC system is consistent with a power law ($\phi(L) dL \propto L^\alpha dL$ with $\alpha = -1.75 \pm 0.07$) down to the 50% completeness limit of the data. At face value, these results do not provide significant evidence to suggest an evolution of the LF from a power law to a Gaussian.

However, the disruption timescales of dynamical effects thought to be responsible for the Gaussian shape of the GC LFs of ‘normal’ galaxies through preferential depletion of low-mass GCs (e.g., Fall & Zhang 2001, hereafter FZ01) depend on galactocentric distance. The stronger tidal field in the central regions does not only yield stronger tidal shocks than in the outskirts, it also imposes a more stringent zero-energy surface on the GCs so that stars can be more easily removed from the GCs through two-body relaxation. Hence, the appearance of a turnover in the GC LF can be expected to first occur in the inner parts of galaxies (see also Gnedin 1997).

With the 1496 GC candidates in our ACS images of NGC 1316, we are now in a position to test this idea for a ~ 3 Gyr-old merger remnant with adequate statistical significance. To this end, we divide the red GC system into two equal-size parts sorted by projected galactocentric radius. For our sample, this division ends up at $85''/2$, or 9.4 kpc from the galaxy center. The result is shown in Fig. 3(c) and (d): The LF of the *outer* half of the red GC system still rises all the way to the detection limit, but *the LF of the inner half of the red GC system shows a clear flattening consistent with a turnover at ~ 1.0 mag fainter than that of the blue GC system.*

We compare these results with predictions of GC disruption models by FZ01 in Fig. 3(e) and (f). The FZ01 models, whose initial GC velocity distribution involves a radial anisotropy which is similar to that of halo stars in the solar neighborhood, show that an initial power-law or Schechter mass function evolves in 12 Gyr to a peaked mass distribution similar to that observed for the Milky Way GC system. To predict the shapes of *luminosity* functions as a function of age, we use the FZ01 model that uses a Schechter initial mass function in combination with the stellar evolution models of Maraston et al. (2001). We use $Z/Z_\odot = 1.0$ for populations of ages 1.5, 3, and 6 Gyr, while we use $Z/Z_\odot = 0.02$ for the 12 Gyr old population, similar to the median metallicity of halo GCs in our Galaxy. Prior to plotting, all resulting LFs were shifted by +0.2 mag so as to let the peak luminosity for the 12 Gyr old, metal-poor model be at $M_V = -7.2$. As Fig. 3(f) shows, the location of the turnover found for the inner half of the red GC system is in remarkably good agreement with those of the FZ01 models for intermediate ages and solar metallicity. It thus seems reasonable to assume that the LF of this second-generation GC system will evolve further to become consistent with the LFs of red GCs in ‘normal’ giant ellipticals.

5. CONCLUSION

We have presented the discovery of a clear flattening consistent with a turnover in the LF of the inner half of the

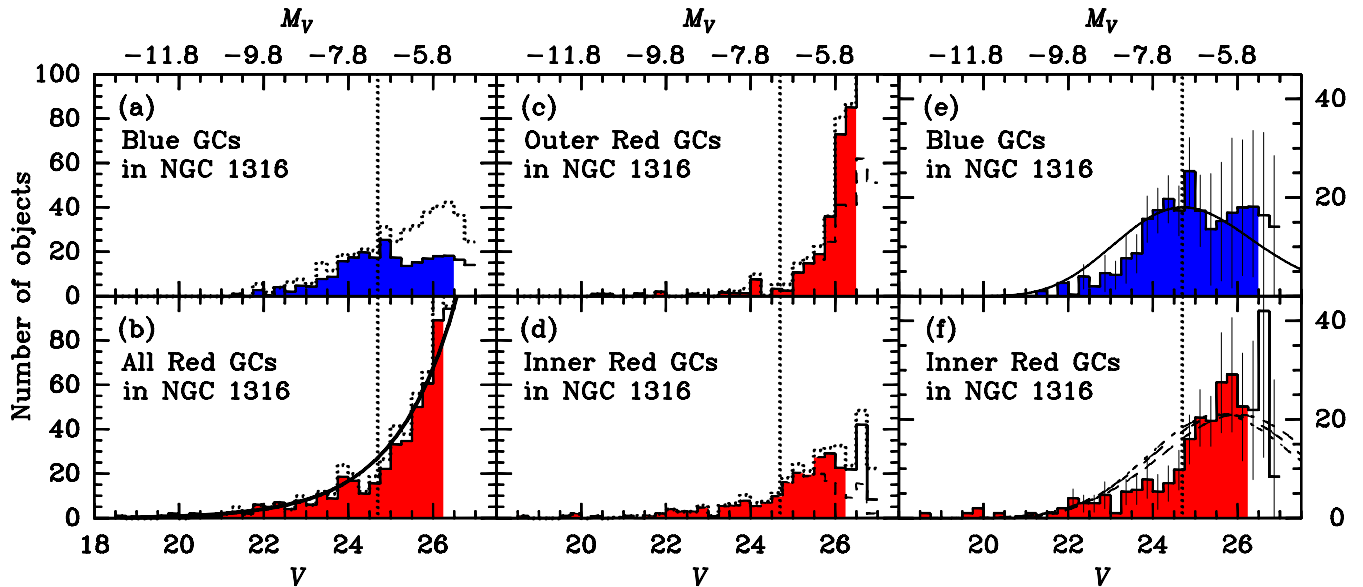


FIG. 3.— V -band luminosity functions (LFs) of GC candidates in NGC 1316. *Panel (a)*: LF of the full blue subsystem. *Panel (b)*: LF of the full red subsystem. *Panel (c)*: LF of the outer 50% of the red subsystem. *Panel (d)*: LF of the inner 50% of the red subsystem. Dashed histograms [only in panels (c) and (d)] mark uncorrected (observed) LFs, dotted histograms mark LFs corrected for incompleteness, and solid histograms mark LFs corrected for completeness and background galaxies. Histograms are filled for magnitude bins brighter than the overall 50% completeness limit of the sample plotted, and open beyond it. The smooth curve in panel (b) is a power-law fit to the LF. The dotted vertical lines represent the predicted turnover magnitude for ‘old’ GC systems (i.e., $M_V = -7.2$). Note the appearance of a flattening consistent with a turnover in the LF of the inner 50% of the red subsystem, which is not present in the outer 50%. *Panel (e)*: Same LF as in panel (a), but at a different scale and with formal errorbars. *Panel (f)*: Same LF as in panel (d), but at a different scale and with formal errorbars. The smooth curves in panels (e) and (f) represent predicted LFs based on a combination of the Fall & Zhang (2001) GC disruption models and the population synthesis models of Maraston et al. (2001). Curves are drawn for the following populations: ages of 1.5 (short-dashed line), 3.0 (long-dashed line), 6.0 Gyr (dash-dotted line), and 12 Gyr (solid line in panel (e)). $Z/Z_\odot = 0.02$ is assumed for the 12 Gyr curve, whereas $Z/Z_\odot = 1.0$ is assumed for the three younger ages. The peak amplitudes of all model curves in panels (e) and (f) are scaled to coincide with those of the underlying histograms.

red, metal-rich GC subsystem of NGC 1316, a ~ 3 Gyr-old merger remnant. The turnover magnitude is consistent with predictions of the Fall & Zhang (2001) models at that age and metallicity. The implication is that the dynamical evolution of metal-rich GC populations formed in gas-rich galaxy mergers *can* change their properties so that they become consistent with the properties of the red, metal-rich GC subsystems that are ubiquitous in ‘normal’ giant ellipticals. This discovery weakens the one remaining argument against the ‘formation by merger’ scenario for the metal-rich GC subsystems in ‘normal’, giant ellipticals, namely that the LFs of GC systems in young and intermediate-age merger remnants are inconsistent

with the Gaussian LFs of old systems. Our results support a picture in which the formation process of giant ellipticals with significant populations of metal-rich GCs was similar to that in gas-rich galaxy mergers observed today.

ACKNOWLEDGMENTS. We thank the anonymous referee for a very constructive review. Support for *HST* Program GO-9409 was provided by NASA through a grant to PG from the Space Telescope Science Institute, which is operated by the Association of Universities for Research in Astronomy, Inc., under NASA contract NAS5-26555.

REFERENCES

- Ashman, K. M., & Zepf, S. E., 1992, *ApJ*, 384, 50
 Baumgardt, H., 1998, *A&A*, 330, 480
 Cohen, J. G., Blakeslee, J. P., & Côté, P., 2003, *ApJ*, 592, 866
 de Grijs, R., Bastian, N., & Lamers, H. J. G. L. M., 2003, *ApJ*, 583, L17
 Fall, S. M., & Rees, M. J., 1977, *MNRAS*, 181, 37P
 Fall, S. M., & Zhang, Q., 2001, *ApJ*, 561, 751 (FZ01)
 Forbes, D. A., Brodie, J. P., & Grillmair, C. J., 1997, *AJ*, 113, 1652
 Forbes, D. A., Beasley, M. A., Brodie, J. P., & Kissler-Patig, M., 2001, *ApJ*, 563, L143
 Geisler, D., Lee, M. G., & Kim, E., 1996, *AJ*, 111, 1529
 Gnedin, O. Y., 1997, *ApJ*, 487, 663
 Goudfrooij, P., Mack, J., Kissler-Patig, M., Meylan, G., & Minniti, D., 2001a, *MNRAS*, 322, 643
 Goudfrooij, P., Alonso, M. V., Maraston, C., & Minniti, D., 2001b, *MNRAS*, 328, 237 (Paper I)
 Harris, W. E., 1996, *AJ*, 112, 1487
 Holtzman, J. A., Faber, S. M., Shaya, E. J., et al. 1992, *AJ*, 103, 691
 Kundu, A., & Whitmore, B. C., 2001, *AJ*, 121, 1888
 Larsen, S. S., Brodie, J. P., Huchra, J. P., Forbes, D. A., & Grillmair, C. J., 2001, *AJ*, 121, 2974
 Maraston, C., Kissler-Patig, M., Brodie, J. P., Barmby, P., & Huchra, J. P., 2001, *A&A*, 370, 176
 Maraston, C., Bastian, N., Saglia, R. P., Kissler-Patig, M., Schweizer, F., & Goudfrooij, P., 2004, *A&A*, 416, 467
 Schweizer, F., 1980, *ApJ*, 237, 303
 Schweizer, F., 1981, *ApJ*, 246, 722
 Schweizer, F., 1987, in: “Nearly Normal Galaxies”, ed. S. M. Faber (Springer: New York), 18
 Schweizer, F., 2002, in: “Extragalactic Star Clusters”, eds. D. Geisler, E. K. Grebel, & D. Minniti (ASP: San Francisco), 630
 Schweizer, F., & Seitzer, P., 1992, *AJ*, 104, 1039
 Schweizer, F., & Seitzer, P., 1998, *AJ*, 116, 2206
 Stetson, P. B., 1987, *PASP*, 99, 191
 van den Bergh, S., 1995, *ApJ*, 450, 27
 Vesperini, E., 2001, *MNRAS*, 322, 247
 Whitmore, B. C., 1997, in: “The Extragalactic Distance Scale”, eds. M. Livio, M. Donahue, & N. Panagia (Baltimore: STScI), 254
 Whitmore, B. C., Zhang, Q., Leitherer, C., Fall, S. M., Schweizer, F., & Miller, B. W., 1999, *AJ*, 118, 1551
 Whitmore, B. C., Schweizer, F., Kundu, A., & Miller, B. W., 2002, *AJ*, 124, 147
 Zepf, S. E., Carter, D., Sharples, R. M., Ashman, K. M., 1995, *ApJ*, 445, L19